Available online at www.sciencedirect.com
SCIENCE DIRECT
International Journal of Heat and Fluid Flow 27 (2006) 167–180
International Journal of HEAT AND FLUID FLOW
www.elsevier.com/locate/ijhff

Optimum natural convection from square cylinder in vertical channel

Khaled Khodary [1], T.K. Bhattacharyya *

Mechanical and Industrial Engineering Department, Indian Institute of Technology Roorkee, Roorkee 247 667, UA, India

Received 8 March 2004; accepted 21 April 2005
Available online 9 November 2005

Abstract

Laminar natural convection from a horizontal isothermal square cylinder inside a vertical adiabatic parallel plate channel is studied using finite difference method. The solution is obtained for the square side length to channel width aspect ratio changed from 0.1 to 0.8. The cylinder is placed at mid-height of the channel at different lateral locations with changeable values for the left to right clearance ratio. The results indicate that the laminar natural convection is significantly affected by the aspect ratio and the lateral position. For any Grashof number, an optimum aspect ratio exists for the maximum heat transfer rate. Central positioning is observed to be the best from the heat transfer point of view. Correlations for the optimum aspect ratio, corresponding Nusselt number and apparent Reynolds number are presented.

Keywords: Natural convection; Numerical; Finite difference; Square cylinder; Channel

1. Introduction

The problem of natural convection in vertical channels with an internal objects is encountered in numerous engineering applications such as heat exchangers, natural circulation boilers, nuclear reactors, solar heating systems, dry cooling towers, and cooling of electronic equipment. In such configurations, the heat released from the internal object decreases the fluid density between the two walls of the channel. This causes a hydrostatic pressure difference between the inlet and exit planes of the channel less than that of the out side fluid. Such pressure imbalance generates the convective flow out from the channel at the upper plane and due to continuity requirement a corresponding inflow at the lower plane. This action is commonly referred as chimney effect. This chimney effect was found to enhance the heat transfer performance more than free space positioning as reported by many scientists.

The problem was investigated numerically and experimentally for different internal object states. Circular cylinder as an internal object has taken the most concern of these studies. In Marsters (1975), the enhancement of average Nusselt number for a single isothermal cylinder between two aluminum walls in comparison with the case of free space positioning was observed even for quite large wall spacing. Enhancements up to 40% and 45% were reported for a single isothermal cylinder confined with two adiabatic walls by Sparrow and Pfeil (1984) and Karim et al., 1986), respectively. The enhancement was found to be accentuated as the internal wall spacing was decreased and as the channel height was increased. No optimal wall-spacing to cylinder-diameter ratio for maximum heat transfer was detected.

* Corresponding author. Tel.: +91 1332 266545.
E-mail addresses: khaledme@iitr.ernet.in, khaledkhodary@yahoo.com (K. Khodary), tapanfme@iitr.ernet.in (T.K. Bhattacharyya).
[1] Present address: Mechanical Power Engineering Department, Faculty of Engineering, Tanta University, Tanta, Egypt.

0142-727X/$ - see front matter © 2005 Elsevier Inc. All rights reserved.
doi:10.1016/j.ijheatfluidflow.2005.04.007

Nomenclature

A	aspect ratio, $A = S/w = 1/W$
g	gravity acceleration (m/s^2)
Gr	Grashof number, $Gr = \frac{g\beta S^3(t_w - t_\infty)}{\nu^2}$
H	channel height (m)
$\hat{H}$	dimensionless channel height, $\hat{H} = H/S$
h	heat transfer coefficient (W/m^2 K)
k	thermal conductivity (W/m K)
L	length of the square cylinder in the experiment (m)
M	dimensionless average induced flow rate, $M = V_{av}W$
Nu	overall average Nusselt number
p	dimensional pressure (N/m^2)
P	dimensionless pressure, $P = p/\rho(\nu/S)^2$
Pr	Prandtl number
R	clearance ratio, $R = X_l{:}X_r$ (Fig. 1)
Ra	Rayleigh number, $Ra = Gr\,Pr$
Re	apparent Reynolds number, $Re = V_{av}$
S	side length of the square cylinder (m) "used as reference length to obtain the non-dimensional parameters"
t	dimensional temperature (K)
T	dimensionless temperature, $T = (t - t_\infty)/(t_w - t_\infty)$
u	dimensional velocity in x-direction (m/s)
U	dimensionless velocity in x-direction, $U = u/(\nu/S)$
v	dimensional velocity in y-direction (m/s)
V	dimensionless velocity in y-direction, $V = v/(\nu/S)$
V_{av}	dimensionless average upward velocity
w	dimensional channel width (m)
W	dimensionless channel width, $W = w/S$
x	distance along horizontal x-axis (m)
X	dimensionless distance along x-axis, $X = x/S$
y	distance along vertical y-axis
Y	dimensionless distance along y-axis, $Y = y/S$

Greeks

β	volumetric expansion coefficient (1/K)
ν	viscous diffusivity (m^2/s)
ρ	density (kg/m^3)

Subscripts

opt	optimum value
w	wall condition
∞	ambient condition

On the other hand, the optimal ratio was suggested by Farouk and Guceri (1982) and Sadeghipour and Razi (2001), but without particular information about this optimal ratio. Moreover, in Konka (2000) the cylinder-diameter to wall-spacing ratio between 0.3 and 0.5 was suggested to be optimal for natural convection from the cylinder confined by two isothermal walls of different temperatures. However, the results of Konka (2000) were obtained for a limited range of low Rayleigh numbers of 600–900 based on the tube diameter.

The vertical isothermal plate as an internal object was studied numerically and experimentally by Naylor and Tarasuk (1993a,b). A maximum enhancement of 200% was predicted by the numerical solution. The horizontal isothermal plate as an internal object was studied numerically by Khaled Khodary and Bhattacharyya (2003), and the convection heat transfer enhancement with an optimal wall-spacing to plate-length ratio was reported. The natural convection in a channel with a built-in square cylinder was studied by Saha (2000) for an isothermal cylinder centrally placed within the channel. This study was limited to a single value of 10 for the ratio of the channel width to the square side length. As such, no optimal ratio was suggested.

It is evident from the literature that the existence of optimal wall spacing to internal object dimension is not resolved comprehensively for circular cylinder, while it has not been investigated for other shapes. Moreover, in spite of the interesting flow patterns associated with many engineering applications of a square cylinder inside channel, this problem has received little attention and related experimental and numerical knowledge is seriously lacking.

In the present work, the laminar natural convection from a square isothermal horizontal cylinder confined by two vertical adiabatic parallel plates is numerically studied. Specifically, the effect of the square-side-length to channel-width aspect ratio and the best lateral position for the cylinder is examined including the possibility of the optimum configuration. Moreover, an experiment is carried out to validate the numerical results and obtain sets of data for natural convection from isothermal square cylinder confined between two insulated walls. Also, a Schlieren optical technique is employed to obtain images of the thermal field around the square cylinder.

2. Formulation and method of solution

The geometry of the problem is depicted in Fig. 1. The present experiments revealed that the flow is steady, laminar and two-dimensional in the range of parameters reported here. Unsteady and three-dimensional flow

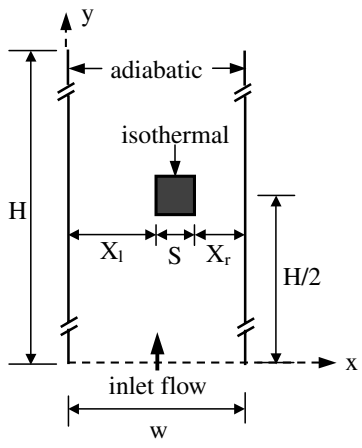

Fig. 1. Problem configuration.

may occur for high Grashof numbers outside the investigated range. Also, viscous dissipation is neglected and Boussinesq approximation is used in the mathematical formulation. Accordingly, the governing equations may be obtained in the following non-dimensional form:

$$\text{Continuity equation}: \quad \frac{\partial U}{\partial X}+\frac{\partial V}{\partial Y}=0 \tag{1a}$$

Momentum and energy equations :

$$\left(U\frac{\partial \Phi}{\partial X}-\lambda\frac{\partial^2 \Phi}{\partial X^2}\right)+\left(V\frac{\partial \Phi}{\partial Y}-\lambda\frac{\partial^2 \Phi}{\partial Y^2}\right)+S_\Phi=0 \tag{1b}$$

where

$$\Phi=U,\ \ \lambda=1,$$
$$S_U=\partial P/\partial X \ \text{ for momentum equation in } X\text{-direction} \tag{1c}$$
$$\Phi=V,\ \ \lambda=1,\ \ S_V=\partial P/\partial Y-Gr\cdot T$$
$$\text{for momentum equation in } Y\text{-direction} \tag{1d}$$
$$\Phi=T,\ \ \lambda=1/Pr,\ \ S_T=0 \ \text{ for energy equation} \tag{1e}$$

The flow enters the channel with a uniform vertical velocity. Its magnitude is developed automatically in the iterative numerical solution. Basically, the average vertical velocity at each iterative step is used as the inlet velocity for the next iterative step. Zero transverse velocity component and ambient temperature are considered at the inlet.

The flow is assumed to come out of the channel smoothly with zero gradients. Due to the unknown details downstream of the channel exit, no unique outlet boundary condition can be fixed. Both zero velocity and temperature gradients and zero curvatures in vertical direction were initially considered as exit conditions. As the results for Nusselt number did not differ by more than 3%, the simpler condition of zero gradients was used at the exit for all reported results here.

The two channel walls are taken to be adiabatic with no-slip flow boundary condition. Finally, isothermal and no-slip flow boundary conditions are used on the surface of the square cylinder.

The boundary conditions are written mathematically in the following non-dimensional forms:

$$\text{At } Y=0 \text{ and } 0\geqslant X\leqslant W: \quad U=0,\ V=V_{\text{av}} \text{ and } T=0 \tag{2a}$$

$$\text{At } Y=\hat{H} \text{ and } 0\geqslant X\leqslant W: \quad \frac{\partial U}{\partial Y}=0,\ \frac{\partial V}{\partial Y}=0 \text{ and } \frac{\partial T}{\partial Y}=0 \tag{2b}$$

$$\text{At } 0\geqslant Y\leqslant \hat{H} \text{ and either } X=0 \text{ or } X=W: \quad U=0,\ V=0 \text{ and } \frac{\partial T}{\partial X}=0 \tag{2c}$$

$$\text{At the outer surface of the square cylinder}: \quad U=0,\ V=0, \text{ and } T=1 \tag{2d}$$

A numerical finite difference scheme based on the Residual Method of Finite Differencing Algorithm given by Bhattacharyya (1997) is used to solve the governing equations. The numerical scheme uses a staggered non-uniform grid and a finite difference formulation by local analytical solution. In brief, Eq. (1) is firstly rearranged in the following residual form:

$$R_P=\frac{\partial U}{\partial X}+\frac{\partial V}{\partial Y} \tag{3a}$$

$$\begin{aligned} R_\Phi &= \left(U\tfrac{\partial \Phi}{\partial X}-\lambda\tfrac{\partial^2 \Phi}{\partial X^2}\right)+\left(V\tfrac{\partial \Phi}{\partial Y}-\lambda\tfrac{\partial^2 \Phi}{\partial Y^2}\right)+S_\Phi \\ &= R_{\Phi,X}+R_{\Phi,Y}+R_{\Phi,S} \end{aligned} \tag{3b}$$

The residues R_P and R_Φ ($\Phi = U$, V and T) are finite difference formulations of the corresponding differential expressions. Local analytical solution is used for finite differencing the combined convection–diffusion terms in R_Φ. This leads to central difference formulation in general, but the diffusion terms are multiplied by factors depending on the cells Peclet number. The finite difference equations are solved using point-iteration and a correction scheme similar as the Newton–Raphson method.

The average upward flow velocity is calculated at each iteration step and used as the inlet upward velocity for the next step. More details are available in Khaled Khodary (2004).

3. Experimental setup and procedures

In order to validate the present numerical results, sets of experimental data were generated for an isothermal square cylinder positioned between two insulated walls. A hollow aluminum square cylinder with 25.7 mm in side length, 2.6 mm in thickness and 53 cm in length

was used. This cylinder was heated, from inside, by cartridge heater, which is controlled by a voltage regulator. The outer surface of the cylinder was highly polished to a mirror finish using buffing and wax compound to reduce the radiation heat losses from the cylinder. To reduce the conduction losses, two Teflon end caps supported the two ends of cylinder. The square cylinder test section was provided with 16 fine copper–constantan thermocouple wires of 0.15 mm in diameter to monitor the wall temperature at various circumferential and axial locations along the outer cylinder surface.

Two thick thermally insulated walls were used to create adiabatic plate channel around the square cylinder test section. The height of the walls was equal to 20 times the outer dimension of the square cylinder. The inner sides of the walls were covered with thin layer of aluminum foil to reduce radiation heat transfer from the square cylinder to the walls. The cylinder and confining walls were mounted between two end glass plates. A steel frame was used to support the assembly. Heat generated in the cylinder test section is dissipated from the surface of the cylinder by convection and radiation.

The convection heat transfer from the cylinder surface Q_{conv} and experimental Nusselt number are calculated as:

$$Q_{conv} = E - Q_{cond} - Q_{rad} = h(4SL)(t_w - t_\infty), \quad Nu = hS/k \tag{4}$$

where E is the measured electrical power input, Q_{cond} is the rate of heat conduction loss from the two end caps, Q_{rad} is the rate of radiation heat transfer and h is the convection heat transfer coefficient. Measurements show that conduction, Q_{cond}, through the end caps is less than 2% of the supplied electrical power.

In the light of Eq. (4), it appears that the accuracy in determining the convective heat transfer rate might well depend on the accuracy of the radiation correction. To avoid this potential difficulty, the apparatus was designed to make $Q_{rad} \ll Q_{conv}$. This was accomplished by the use of highly polished aluminum surface for the square cylinder and aluminum foil for the inner surface of the shrouding walls. The results of radiation calculation showed that the maximum Q_{rad} was 8% of E.

The experimental arrangement allowed a range of temperature difference $(t_w - t_\infty)$ from 1.4 °C to 136.3 °C. The uncertainty in the resultant experimental Nusselt number was found to have a maximum value of 10% at $(t_w - t_\infty) = 1.4$ °C. However, this uncertainty decreases with increasing the temperature difference to reach 0.6% at $(t_w - t_\infty) = 136.3$ °C. The experimental and numerically predicted Nusselt numbers were compared. Excellent agreement was found as shown later.

A Schlieren optical system was used to produce images containing information on the temperature field around the square cylinder inside the channel. The system consists of a vapor mercury lamp as a light source, two concave mirrors, a small reflecting mirror and a viewing screen. A digital camera of 3.2 Mega pixel resolution was used to record the generated image on the viewing screen. More details for the present experiment are available in Khaled Khodary (2004).

4. Results and discussion

Experiments were performed considering the aspect ratio, A, the clearance ratio, R, and the Grashof number, Gr as variable parameters. Both A and R were controlled by adjusting the location of the two insulated walls with respect to the internal square cylinder, while different values of Gr were obtained by adjusting the power input. The experiment facilitated a range of Grashof number from 3700 up to 1.39×10^5. The main results from the experiments are the Nusselt numbers and Schlieren images for thermal pattern inside the channel. Also, as a prelude to the results for the confined cylinder, measurements were obtained for the case of the cylinder in free space positioning.

Numerical solutions are obtained for air of $Pr = 0.72$ as a working medium, different aspect ratios ranging from 0.1 to 0.8, values of Grashof number between 1 and 3×10^6, and discrete values of the clearance ratio of 1:1, 3:2, 3:1, 5:1 and 1:0. The cylinder is situated at the mid-height of the channel. The channel height is fixed with a value equal to 20 times the length of a side of the square section. However, the effect of the channel height is also tested for some cases. It was found that, the heat transfer rate increased as the channel height was increased. This is in agreement with Sparrow and Pfeil (1984) for a confined circular cylinder.

Grid independent test and convergence test are carried out for each value of A and R reported here. No common grid is used for all problems. The convergence is decided when the percentage change in the resulted average upward velocity V_{av} is less than 10^{-6} for two successive iterations. Convergence of the basic variables U, V, P and T is checked as well using fractional changes less than 10^{-5} for two successive iterations with respect to their absolute values. Table 1 shows the convergence characteristics and effect of grid size for a typical case.

4.1. Schlieren images and numerical isotherms

Figs. 2 and 3 show the Schlieren images in the central and off-central positioning of the cylinder inside the channel for aspect ratios $A = 0.2$ and $A = 0.5$ respectively. Both figures represent the thermal field around the square cylinder inside the channel for high values of Grashof numbers. The two figures obviously show that the field inside the channel is steady, laminar and two dimensional for both central and off-central posi-

Table 1
Convergence performance and grid independent test for $A = 0.4$, $R = 1{:}1$ and $Gr = 10^4$

Iteration no.		501	1001	1501	2001	2501	3001	3501	4001	4501	5001	5501	5764
Grid size (58×180)	V_{av}	190.42	187.34	189.25	189.05	189.07	189.12	189.12					
	Nu	5.56	5.59	5.60	5.60	5.60	5.60	5.60					
Grid size (64×200)	V_{av}	173.01	185.34	187.60	187.43	187.67	187.68	187.74	187.75	187.77	187.78	187.78	187.79
	Nu	5.41	5.51	5.55	5.55	5.55	5.55	5.55	5.55	5.55	5.55	5.55	5.55

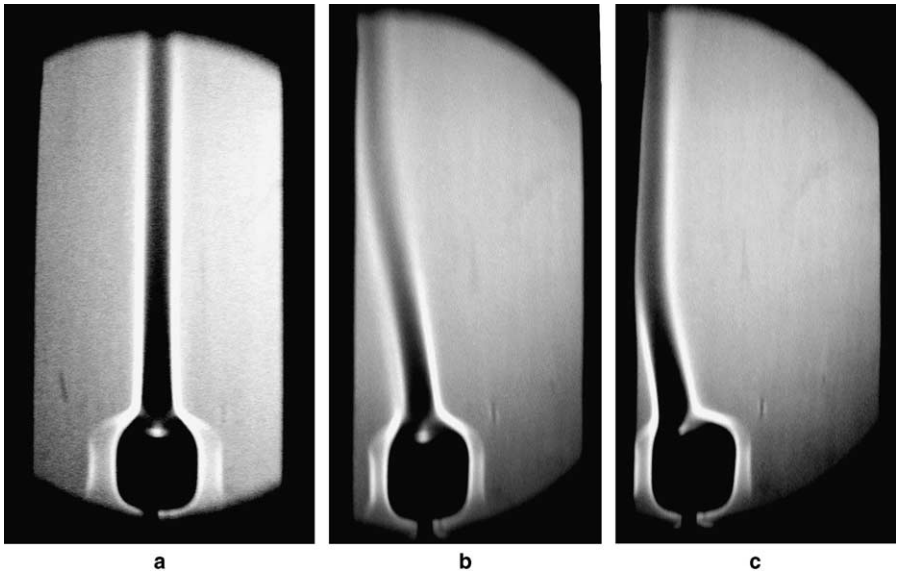

Fig. 2. Schlieren images for aspect ratio 0.2: (a) $R = 1{:}1$ and $Gr = 1.3 \times 10^5$, (b) $R = 1{:}1$ and $Gr = 1.3 \times 10^5$, (c) $R = 1{:}5$ and $Gr = 1.2 \times 10^5$.

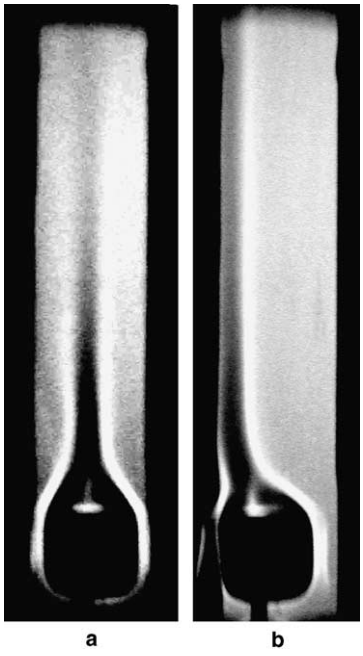

Fig. 3. Schlieren images for aspect ratio 0.5: (a) $R = 1{:}1$ and $Gr = 1.2 \times 10^5$, (b) $R = 1{:}3$ and $Gr = 1.3 \times 10^5$.

tioning of the cylinder. In the case of $A = 0.2$ and central positioning as shown in Fig. 2(a), the channel walls are considerably far away from the thermal boundary layer around the cylinder. So, in spite of the lateral shifting of the cylinder, the nearest confining wall was still far away to directly influence the thermal boundary layer around the cylinder. However, for low values of Grashof number, the thermal boundary layer is expected to be thicker. In this case the nearest confining wall may influence the thermal boundary layer around the cylinder. On the other hand, for the case of $A = 0.5$ as shown in Fig. 3, the channel is narrow and an interference between the confining wall and the thermal boundary layer around the cylinder is possible even for the central positioning ($R = 1{:}1$). So, slight lateral shifting of the cylinder considerably influences the thermal boundary layer around the cylinder and consequently the average Nusselt number is changed.

For qualitative comparison between the present numerical and experimental results, numerical solutions are obtained for the same cases presented in Fig. 2. The isothermal lines are presented in Fig. 4. Comparing Figs. 2 and 4, it can be seen that the characteristics of isothermal lines numerically obtained are in excellent

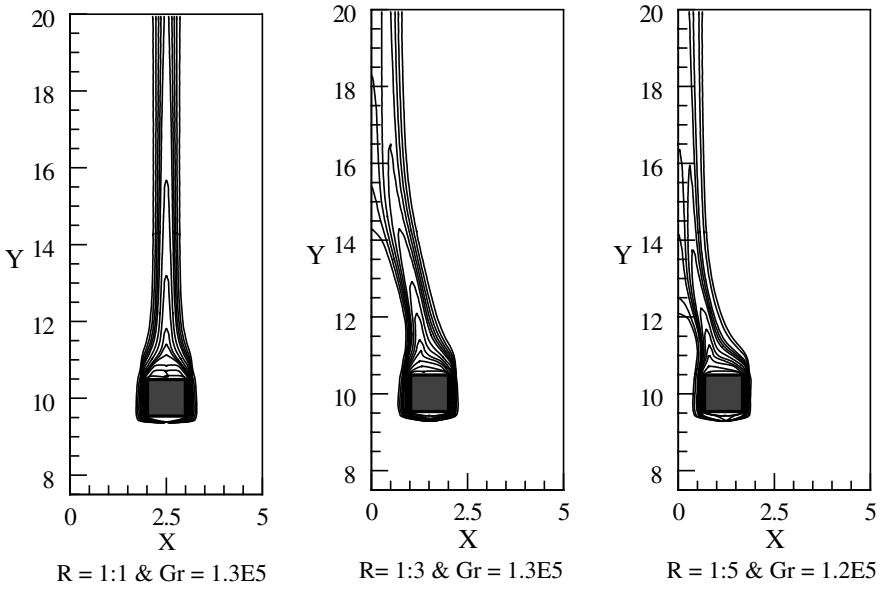

Fig. 4. Isothermal lines for aspect ratio 0.2 and different R.

agreement with the thermal patterns shown by the Schlieren images.

4.2. Flow and thermal patterns

4.2.1. Central lateral position inside the channel

Fig. 5 depicts the numerically obtained streamlines and the isotherms for $A = 0.4$, $R = 1{:}1$ and different values of Grashof numbers. The left half of the figure represents the streamlines while the right half represents the isotherms. Similar patterns for other values of aspect ratio are obtained. The figure shows that the flow and thermal patterns depend considerably on the Grashof number. At low values of Grashof number the induced flow moves upward making a smooth turn around the hot square cylinder. Increasing the Grashof number resulted in the induced flow intensified. A recirculation zone above the upper surface of the hot square cylinder

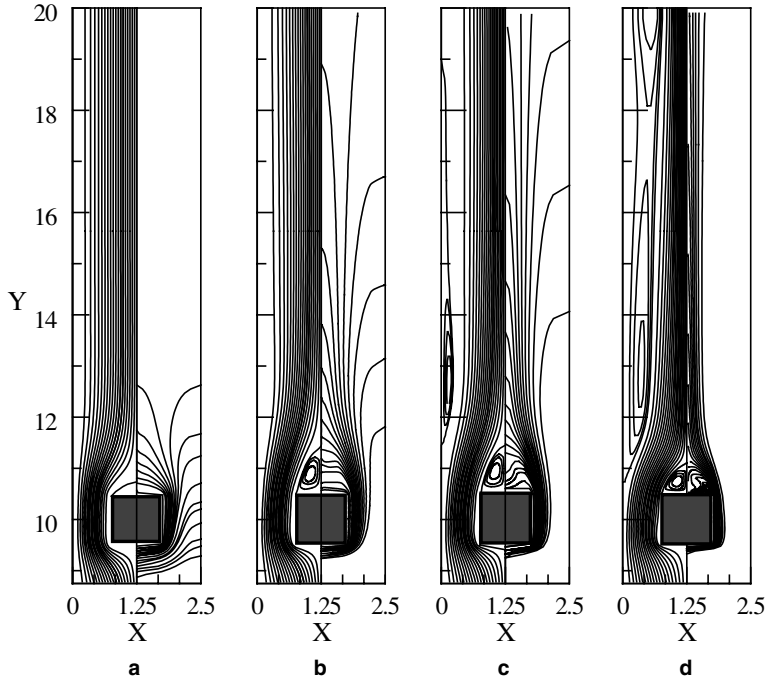

Fig. 5. Streamlines isotherms for central lateral position, $A = 0.4$ and different Gr: (a) $Gr = 100$, (b) $Gr = 2000$, (c) $Gr = 10^4$ and (d) $Gr = 5 \times 10^5$.

occurs. Then other recirculating zones adjacent to the channel walls are created and grow with the Grashof number until they become open sided at the channel exit plane.

The dimensionless height of the recirculation zone above the topside of the square cylinder, $\hat{H}_{recir}$, is represented in Fig. 6. As it is clear from the figure, for values of $A > 0.2$ the height of this recirculation zone increases with Grashof number till some limit and then it decreases. This may be attributed to the compression of this zone due to the expansion of the two recirculation zones adjacent to the walls. For $A < 0.2$ this retardation on recirculation zone was not found.

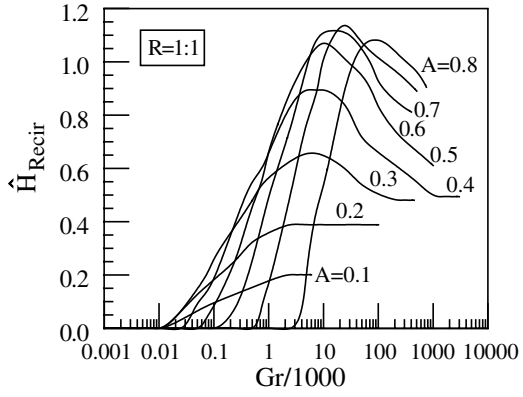

Fig. 6. Height of the recirculation zone above the square cylinder.

As Fig. 5 shows, at low values of Grashof number the isotherms to the body trace closed paths. At low values of Grashof number there are considerable gaps between the isotherms and also large gap between the lowest value isotherm and the bottom of the cylinder. This is clearly due to the axial diffusion of heat, which can propagate towards the channel inlet plane and increase the temperature of the fluid above the ambient even before it reaches the hot body. With increasing the Grashof number, the isotherms upstream of the cylinder become more compact and closer to the bottom of the square cylinder. Moreover, some of the isotherms will leave the closed paths and make a plume downstream of the cylinder. These patterns continue until the isotherms have dips in the middle region above the upper surface of the square cylinder, Fig. 5(c) and (d), and a plume in the wake region downstream the hot cylinder is formed at high values of Grashof number. This dip shape of isotherms is due to the strong recirculation zone above the cylinder that suppresses the diffusion effect causing less downward thermal penetration while it enhances the convection effect.

4.2.2. Off-central lateral position inside the channel

Fig. 7 depicts the streamlines and isotherms for off-central positions of the cylinder and for Grashof number of 10^4. The streamlines and isotherms for central position and for the same A and Gr are represented in Fig. 5(c). When shifting the cylinder towards the channel's right wall, both the streamlines and isotherms slant

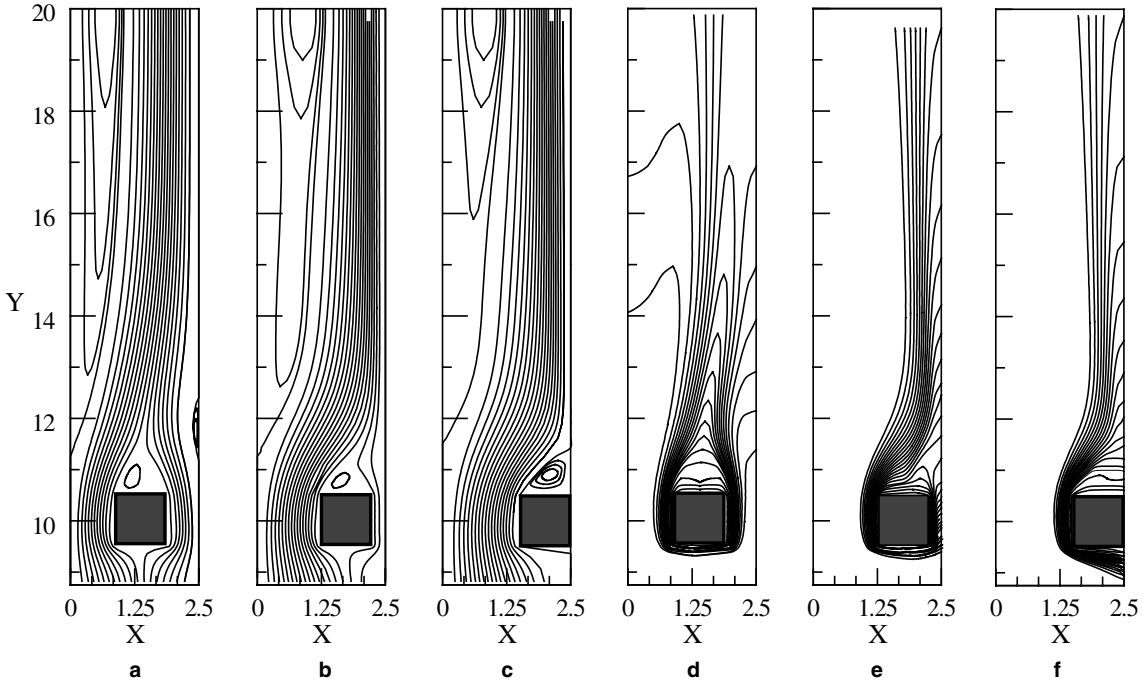

Fig. 7. Streamlines and isotherms for $A = 0.4$, $Gr = 10^4$ and different R: (a–c) streamlines for $R = 3{:}2$, 5:1 and 1:0 resp., (d–f) isotherms for $R = 3{:}2$, 5:1 and 1:0 resp.

towards the same right direction. The recirculation zone adjacent to the left wall widens and the right one is compressed till it vanishes. This means that the flow is intensified in the left side, and it accelerates the occurrence of the flow instability as mentioned before. For a wall-attached cylinder, flow separation occurs downstream behind the square cylinder. As the cylinder approaches the right wall, the isotherms in the left side leave the wall and extend through the plume while more closed paths are formed in the right side.

4.3. Limits of Grashof number used

4.3.1. Central lateral position inside the channel

It should be mentioned that the calculations are carried out for *Gr* between two limiting values. The lower limit may be called as conduction limit. It is detected when a sensible temperature gradient occurs at the channel inlet plane. Below this limit the axial diffusion of heat which propagates downward from the hot cylinder reaches the channel inlet plane. The upper limit of Grashof number may be called as laminar stability limit above which the flow becomes oscillatory or three-dimensional. The present numerical method is itself capable of identifying this upper limit. This is because the method is based on steady-state equations, which makes convergence is not possible with any grid if a steady-state solution does not exist.

All results presented here lie within the range between these two limits. For central lateral positioning of isothermal square cylinder, Fig. 8 shows a graphical representation for these two limits versus aspect ratio. As shown in the figure, the two limits are affected by aspect ratio. The early oscillatory flow in the wide channel is attributed to the faster formation and growth of the recirculation zones adjacent to the wall than the case of narrow channel. The narrow channel apparently provides more stable flow than a wide channel for natural convection from internal bodies.

4.3.2. Off-central lateral position inside the channel

Calculations show that, lateral shifting of the square cylinder inside the channel has dissimilar effects on the two limits of Grashof number. The lower limit is slightly affected while the upper limit is significantly reduced for the same *A*. This may be explained by considering the change that happens to the flow pattern inside the channel. As seen earlier, shifting the cylinder towards one channel wall widens the recirculation zone adjacent to the other channel wall. This accelerates the occurrence of flow oscillation and instability.

4.4. Induced upward flow and apparent Reynolds number

4.4.1. Central lateral position inside the channel

It is well known that the induced upward flow inside the channel is generated due to the buoyant effect of the hot cylinder inside the channel. Calculations show that, for all investigated values of aspect ratio, the total average induced upward flow rate increases with the Grashof number. The dimensionless average induced flow rate through the channel versus Grashof number for different aspect ratios and central positioning of the square cylinder is depicted in Fig. 9.

In order to evaluate the strength of the flow across the square cylinder, the apparent Reynolds number, *Re*, was determined on the basis of average upward velocity and the square cylinder dimension ($Re = V_{av} = MA$). As expected, the strength of the flow was found to increase with the increase of Grashof number. The apparent Reynolds number raised to power of 0.25 was found to be linearly dependent on the logarithm of Grashof number with average deviation of 1.5%. Corre-

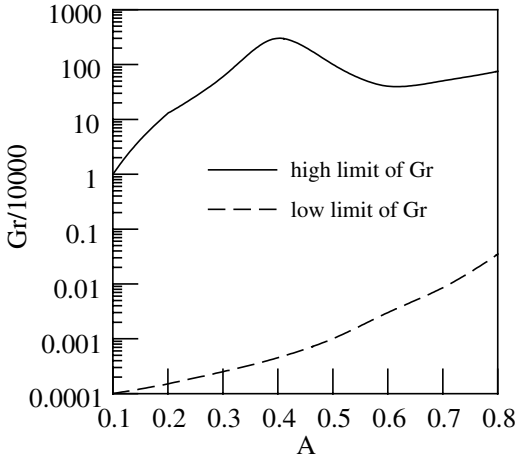

Fig. 8. High and low limits of *Gr*.

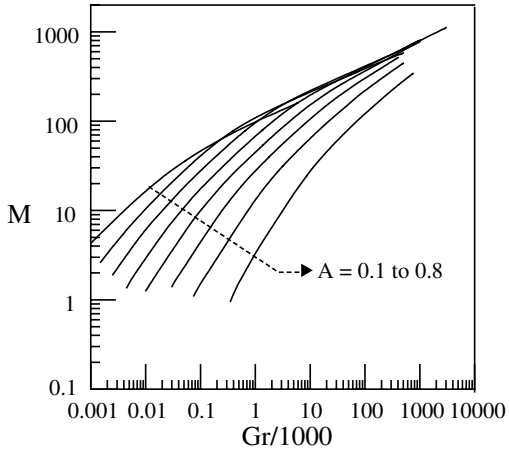

Fig. 9. *M* versus *Gr* for $R = 1{:}1$.

lation for Re is shown in Eq. (5) in which values of E_1 and E_2 are listed in Table 2.

$$Re^{0.25} = E_1 \ln(Gr) + E_2 \quad (5)$$

The apparent Reynolds number versus the aspect ratio is presented in Fig. 10. It is clear that for each Grashof number there is one aspect ratio at which the strength of the flow across the square cylinder is maximum.

4.4.2. Off-central lateral position inside the channel

Fig. 11 depicts the effect of shifting the cylinder towards the wall on the total average induced flow rate through the channel for different aspect ratios. For all values of A, the average induced flow monotonically increases with the Grashof number irrespective of the value of R. The figure clearly shows that for low values of aspect ratio ($A = 0.2$), the induced flow is decreased when the cylinder shifts towards the wall. This effect increases with values of Grashof number and becomes considerable at high values of Grashof number. For large values of aspect ratio, the induced flow is decreased by shifting the cylinder for high values of Grashof number while it is accentuated for low values of Grashof number. Significant effect at low values of Grashof number is noticeable for $A = 0.7$.

Table 2
Values E_1 and E_2 for Eq. (5)

A	E_1	E_2
0.1	0.1398	0.8117
0.2	0.1904	0.7937
0.3	0.2346	0.6529
0.4	0.2795	0.3610
0.5	0.3157	0.0455
0.6	0.3432	−0.3058
0.7	0.3729	−0.7915
0.8	0.4105	−1.5674

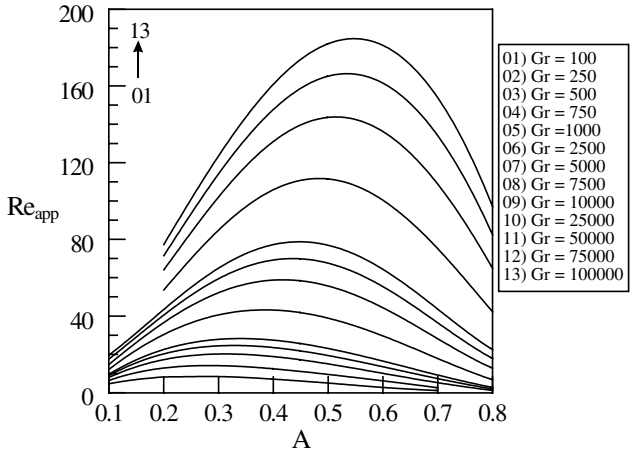

Fig. 10. Re versus A for $R = 1{:}1$.

An interesting result for the ratio by which the flow is divided in the two clearance gaps at left and right sides of the cylinder is presented in Fig. 12. The figure depicts the left to right flow ratio versus the Grashof number for the aspect ratio of $A = 0.4$. For symmetrical lateral position of the cylinder, the flow is divided equally, and this fact is logical. When shifting the cylinder towards the right wall, the flow is divided with the ratio which depends on A, R and Gr. For low values of Grashof number, the flow is weak and most of the flow takes the less resistant path from the wide left gap resulting in flow-dividing ratio considerably higher than the available area ratio or R. For increasing Grashof number the flow becomes stronger and a higher percentage of the flow penetrates through the narrow right gap which reduces the flow-dividing ratio until it approaches a value near R. This result gives further explanation for the flow intensity and growth of the recirculation zone in the left side.

4.5. Average Nusselt number

4.5.1. Central lateral position inside the channel

The average Nusselt number over the square cylinder was calculated by integrating the local Nusselt number over the cylinder surface. Before discussing the characteristics of the Nusselt number, comparison with those obtained experimentally in the present investigation is made for validating the numerical results. As shown in Fig. 13 for different values of aspect ratios. For the case of aspect ratio 0.2, the numerical and experimental results are in close agreement. On the other hand, for the case of higher aspect ratio, the predicted Nusselt numbers by numerical procedure are found to be slightly higher than the experimental Nusselt number with a maximum deviation of about 8% at $A = 0.7$. This deviation is probably due to enhanced unaccounted heat losses in experiment when the internal object is very close to the walls of the channel.

The average Nusselt numbers obtained numerically and experimentally for different values of Grashof number, aspect ratio and central lateral positioning of the cylinder are shown in Fig. 14. It is clear that the Nusselt number increases with the Grashof number for all aspect ratios while for a constant value of Grashof number the Nusselt number may decrease or increase with change in the aspect ratio. The figure shows specific information that, for each value of Grashof number, one value of aspect ratio gives the maximum Nusselt number. The similarity between the experimental and numerical results in the existence and trend of optimum aspect ratio is obvious in the figure.

Referring to Fig. 10 and comparing with Fig. 14, the analogy between the momentum and heat transfer mechanisms may be noted. This establishes the fact of the existence of an optimum configuration for maximum natural convection in the present configuration.

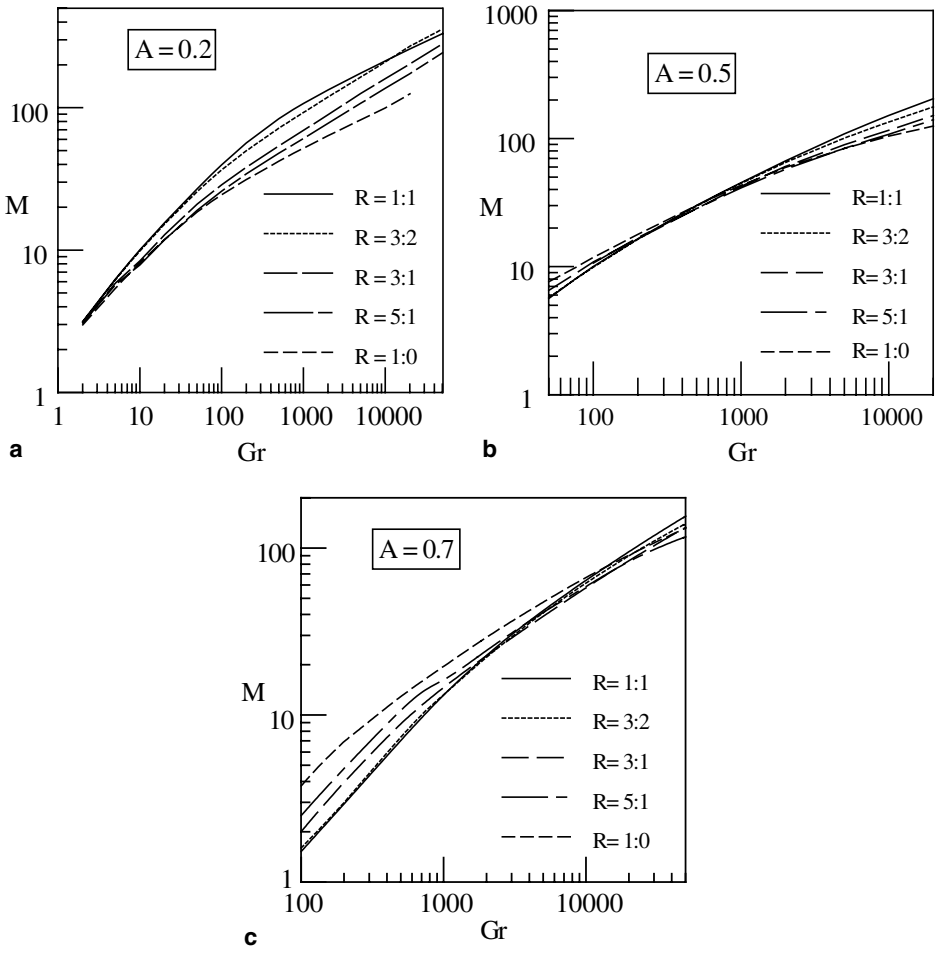

Fig. 11. M versus Gr for different A.

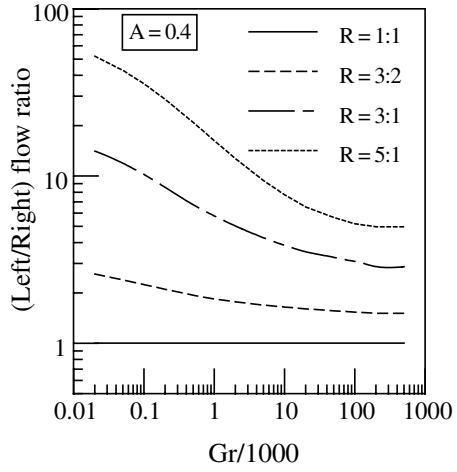

Fig. 12. Left to right flow ratio versus Gr for $A = 0.4$.

Also, from Fig. 14 the reason for the doubt in the literatures about the existence of optimum aspect ratio may be explained. Literatures which suggested the existence of optimum aspect ratio were mostly investigating the problem for low values of Grashof number, in which an optimum aspect ratio may be easily observed as shown in the figure. On the other hand, literatures that did not show optimum aspect ratio were mostly investigating the problem for high values of the Grashof number, in which optimum value for aspect ratio may not be possible to observe. As a specific example, in Sparrow and Pfeil (1984) a range of aspect ratio lower than 0.667 and the Rayleigh number ranging from 1.5×10^4 to 2×10^5 (equivalent to a Grashof number range from about 2×10^4 to 2.8×10^5 assuming a Prandtl numbers of 0.72) were investigated.

Another representation for the predicted Nusselt number versus the Grashof number and for some selected values of aspect ratios is shown in Fig. 15. Typical characteristics existed for other values of aspect ratio. As clear from the figure, each curve has two asymptotes and may be expressed by the following:

$$\text{Lower asymptote } Gr \to 0: \quad Nu \to C_1\, Gr^{N_1} \tag{6a}$$

$$\text{Upper asymptote } Gr \to \infty: \quad Nu \to C_2\, Gr^{N_2} \tag{6b}$$

Values of C_1, C_2, N_1 and N_2 are obtained by fitting the available numerical results. These values are tabulated

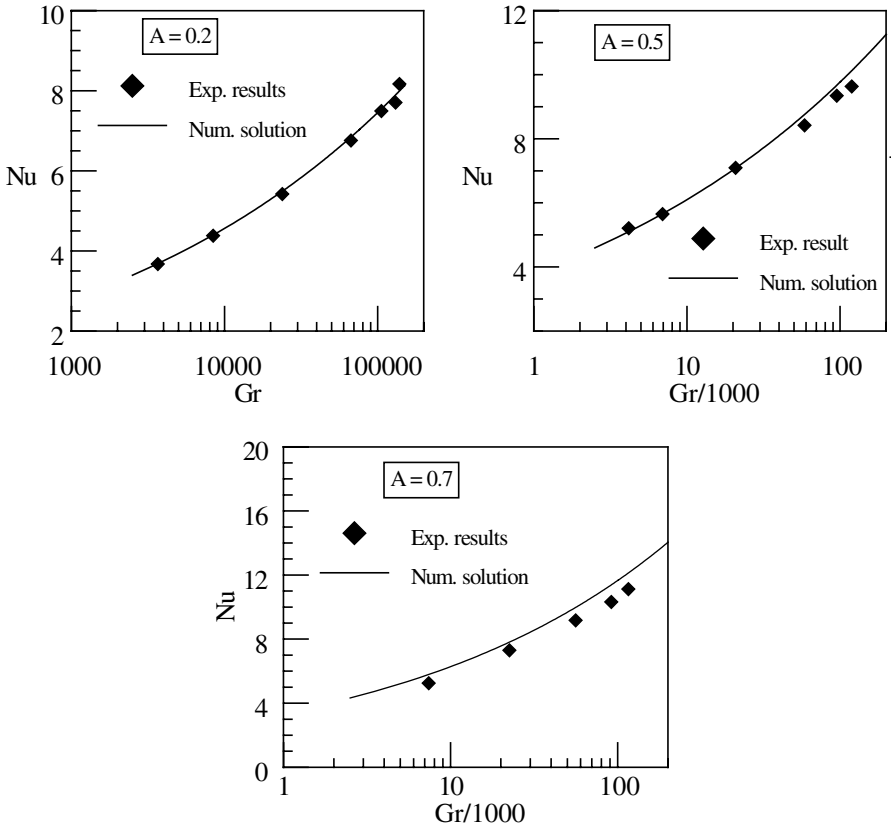

Fig. 13. Comparison between numerical and experimental *Nu* for $R = 1{:}1$.

in Table 3 for different aspect ratios. It is interesting to know that, numerous literatures like Elenbass (1942), Raithby and Hollands (1975), and Martin et al. (1991), have established similar two asymptotes for the free convection between two heated vertical plates. These two limits were referred as the fully developed limit and single plate limit. Moreover, in Naylor and Tarasuk (1993a), these two limits have been established for the vertical plate inside a channel and referred as the fully developed limit and isolated plate limit. In the present configurations the two limits may also be referred to the fully developed limit and unconfined cylinder limit.

Churchill and Usagi (1972) proposed a method for correlating such types of two asymptotes which is commonly found in heat and mass transfer problems. According to the procedure of such method, a correlation is obtained in the form of Eq. (7) for each case of aspect ratio. While the values of N for the whole individual aspect ratios can be collected and correlated as given in (8). The average deviation is 1.68% and the maximum deviation is 5.87% for the correlations of *Nu* presented here.

$$Nu = [(C_1\, Gr^{N_1})^{-N} + (C_2\, Gr^{N_2})^{-N}]^{-1/N} \tag{7}$$

$$N = 1.606A^{-0.8387} \tag{8}$$

4.5.2. Off-central lateral position inside the channel

The numerically predicted average Nusselt numbers over the square cylinder for different values of aspect ratio are illustrated in Fig. 16. Examination of the figure shows that the average Nusselt number increases monotonously with Grashof number for all values of R. It can be clearly seen from the figure that the average Nusselt number is sensitive to the cylinder lateral position. More specifically, calculation shows that, shifting the cylinder towards the wall generally leads to heat transfer degradation. This observation is also supported by the experimental results represented in Fig. 17. On the other hand, Fig. 16 shows that, for the cases of large values of A and low values of Gr, heat transfer augmentation may occur when the cylinder is shifted towards the wall.

4.6. Optimization

From the discussion on the result of average Nusselt number versus aspect ratio, clearance ratio and Grashof number, it can be observed that:

- For channel with small aspect ratio, symmetrical lateral position of the cylinder gives values of Nusselt number higher than the off-central positions for the investigated range of Grashof number.

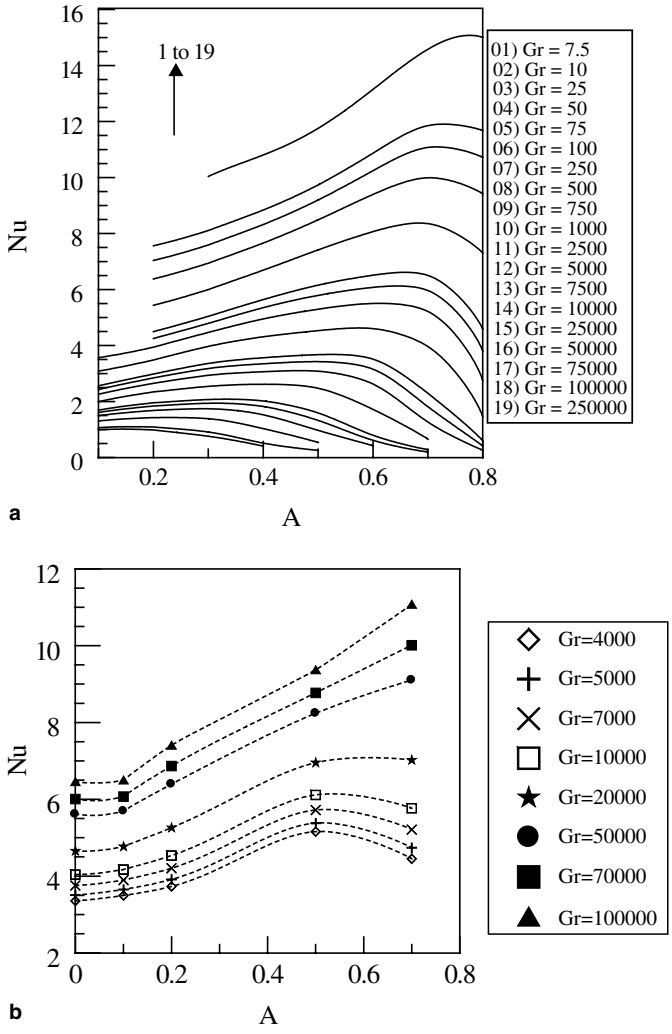

Fig. 14. *Nu* versus *A* for different *Gr*: (a) numerical and (b) experimental.

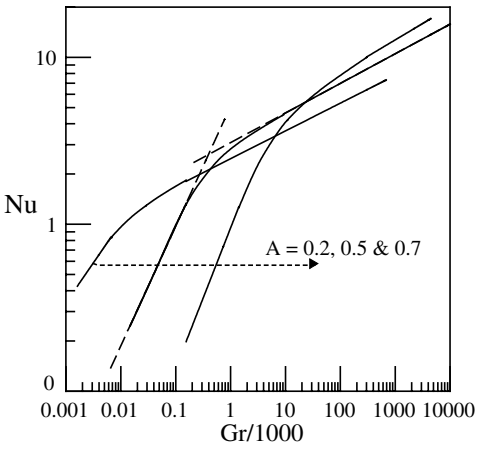

Fig. 15. *Nu* versus *Gr* for different *A*.

Table 3
Coefficient C_1, C_2, N_1 and N_2

A	C_1	N_1	C_2	N_2
0.1	0.5291	0.3214	0.7343	0.1808
0.2	0.3397	0.5570	0.7823	0.1941
0.3	0.1677	0.7494	0.8239	0.2003
0.4	0.0805	0.7931	0.8226	0.2093
0.5	0.0359	0.8373	0.9062	0.2068
0.6	0.0110	0.9288	0.8687	0.2191
0.7	0.0029	0.9795	0.8448	0.2289
0.8	0.0003	1.1001	0.6959	0.2471

- For channel with large aspect ratio, the above observation is also true except for low values of Grashof number where the reverse trend is found. However for these circumstances the Nusselt numbers for central positioning or even the augmented one for off-central positioning are considerably smaller than the Nusselt numbers with less aspect ratio.

A comparative examination indicates that, for any value of Grashof number and suitable value of aspect ratio, the symmetrical lateral positioning is the best for

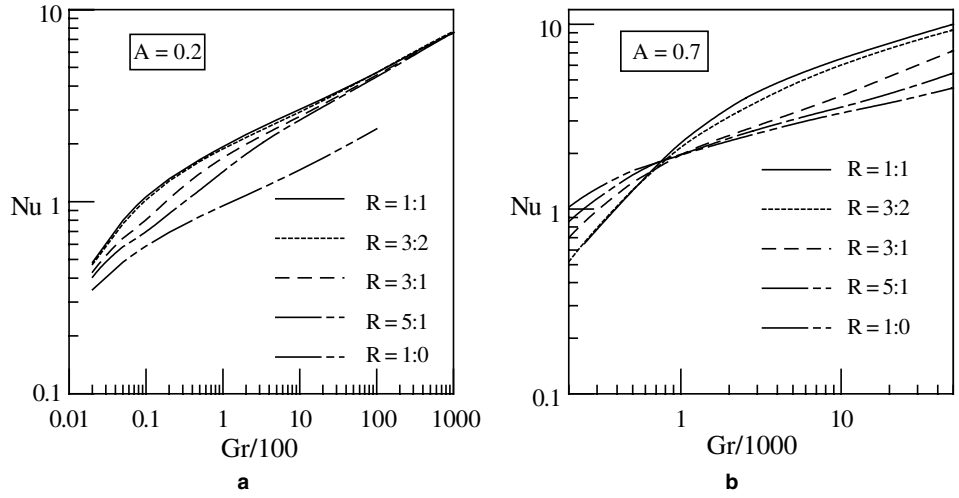

Fig. 16. Numerical average Nusselt number for off-set cylinder positioning.

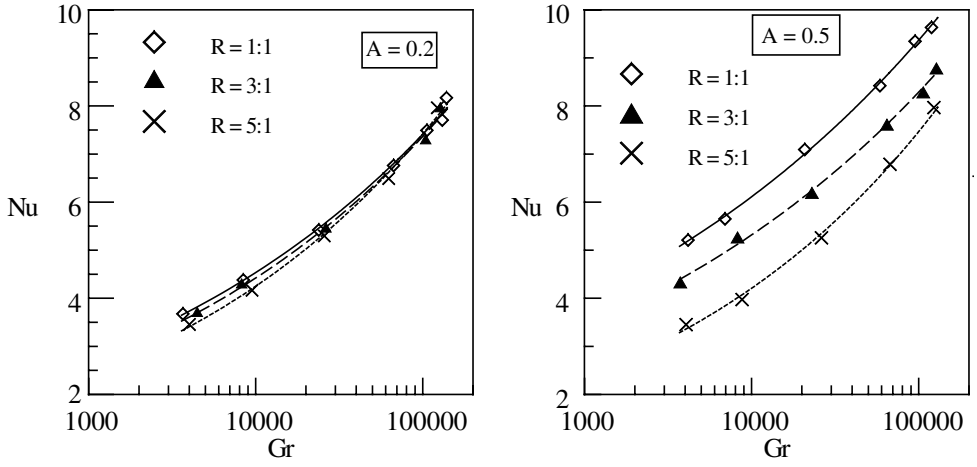

Fig. 17. Experimental average Nusselt number for off-set cylinder positioning.

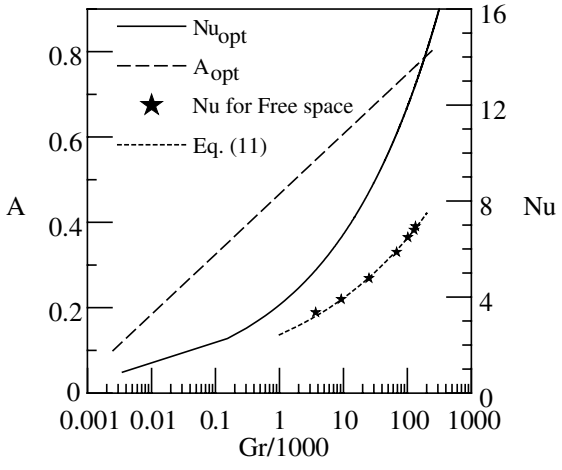

Fig. 18. Optimum *Nu* and optimum *A* versus *Gr*.

maximum Nusselt number. On the other hand, Fig. 14 shows that for symmetrical positioning and for each specific value of Grashof number, an optimum aspect ratio exists for the maximum Nusselt number. A collecting of these optimum values of aspect ratio and corresponding optimum Nusselt number is represented in Fig. 18. Both the optimum aspect ratio and corresponding optimum Nusselt number are found to be well correlated by Eqs. (9) and (10), respectively.

$$A_{\text{opt}} = 0.0433 + 0.0612\text{Ln}(Gr) \tag{9}$$

$$Nu_{\text{opt}} = 0.625Gr^{0.256} \quad Gr \geqslant 2.5 \tag{10}$$

Finally, apparent Reynolds Number corresponding to the optimum aspect ratio may be obtained from Eq. (5) and Table 2.

Fig. 18 also include representation of Nusselt number obtained from the present experiment for the case of cylinder in free space positioning. This present

experimental result spanned the range of Grashof number from about 3.7×10^3 to almost 1.3×10^5 and very well represented by the correlation (11). The average deviation between the correlation and the actual collected experimental data is 1.25% and the maximum deviation is 1.95%.

$$Nu = 0.617 Gr^{0.204} \tag{11}$$

The advantage of using two walls for confining a hot object on the heat transfer rate from the object is clear from the figure. For example, an enhancement of average Nusselt number of 86.8% at Grashof number of 1.3×10^5 is obtained due to the effect of confining walls around the hot square cylinder.

5. Conclusions

Steady laminar natural convection from horizontal hot square cylinder under uniform surface temperature, and positioned between two vertical adiabatic parallel plates is investigated numerically and compared with experiment. The problem is quantitatively as well as qualitatively examined for air as a working medium, channel height to square side length of 20, aspect ratio A varied from 0.1 to 0.8 and different lateral locations of the cylinder. Results are obtained for values of Grashof number between 1 and 3×10^6. The following observations can be made from the investigation:

1. Central lateral positioning of the cylinder inside the channel is the best from the heat transfer point of view.
2. There exists an optimum aspect ratio for maximum Nusselt number in the present configuration.
3. For given Grashof number, the optimum aspect ratio can be calculated using Eq. (9).
4. The maximum Nusselt number when the optimum aspect ratio is used may be calculated by Eq. (10).
5. The corresponding apparent Reynolds number when optimum aspect ratio is used may be calculated by Eq. (5).
6. For a given aspect ratio, the variation of Nusselt number versus Grashof number shows two asymptotes. Nusselt number may be correlated as given in Eqs. (7) and (8).
7. An enhancement of the average Nusselt number of 86.8% at Grashof number of 1.3×10^5 is observed for the square cylinder due to shrouding by a channel.

References

Bhattacharyya, T.K., 1997. Free convection in channel—an alternative numerical approach and illustrations. Commun. Numer. Methods Eng. 13, 387–396.

Churchill, S.W., Usagi, R., 1972. A general expression for the correlation of rates of transfer and other phenomena. AIChE J. 18 (6), 1121–1128.

Elenbass, W., 1942. Heat dissipation of parallel plate by free convection. Physics 9, 1–28.

Farouk, B., Guceri, S.I., 1982. Natural and mixed convection heat transfer around a horizontal cylinder within confining walls. Numer. Heat Transfer 5, 329–341.

Karim, F., Farouk, B., Namer, I., 1986. Natural convection heat transfer from a horizontal cylinder between vertical confining adiabatic walls. ASME J. Heat Transfer 108, 291–298.

Khaled Khodary Esmaeil, 2004. Natural convection from off-centered object in a vertical channel. Ph.D. thesis, Indian Institute of Technology Roorkee, Roorkee 247 667, UA, India.

Khaled Khodary, Bhattacharyya, T.K., 2003. Natural convection from off-centered horizontal plate inside a vertical channel. In: Proceedings of ISME-XIII National Conference of Indian Society of Mechanical Engineers, December 30–31, IIT Roorkee, Paper number: TH-047.

Konka, W.T., 2000. Natural convection heat transfer around horizontal tube in vertical slot. Int. J. Heat Mass Transfer 43, 447–455.

Marsters, G.F., 1975. Natural convection heat transfer from a horizontal cylinder in the presence of nearby walls. Can. J. Chem. Eng. 53, 144–149.

Martin, L., Raithby, G.D., Yovanovich, M.M., 1991. On the low Rayleigh number asymptote for natural convection through an isothermal, parallel-plate channel. ASME J. Heat Transfer 113, 899–905.

Naylor, D., Tarasuk, J.O., 1993a. Natural convective heat transfer in a divided vertical channel: Part I—numerical study. ASME J. Heat Transfer 115, 377–387.

Naylor, D., Tarasuk, J.O., 1993b. Natural convective heat transfer in a divided vertical channel: Part II—experimental study. ASME J. Heat Transfer 115, 388–394.

Raithby, G.D., Hollands, K.G.T., 1975. A general method of obtaining approximate solutions to laminar and turbulent free convection problems. Adv. Heat Transfer 11, 265–315.

Sadeghipour, M.S., Razi, Y.P., 2001. Natural convection from a confined horizontal cylinder: the optimum distance between the confining walls. Int. J. Heat Mass Transfer 44, 367–374.

Saha, A.K., 2000. Free convection in a vertical channel with a built-in heated square block. In: Proceedings of the 4th ISHMT-ASME Heat Mass Transfer Conference and 15th National Heat Mass Transfer Conference, India, pp. 533–538.

Sparrow, E.M., Pfeil, D.R., 1984. Enhancement of natural convection heat transfer from a horizontal cylinder due to vertical shrouding surface. ASME J. Heat Transfer 106, 124–130.